HHS Public Access

Author manuscript

J Vasc Interv Radiol. Author manuscript; available in PMC 2021 October 01.

Published in final edited form as:

J Vasc Interv Radiol. 2020 October ; 31(10): 1612–1618.e1. doi:10.1016/j.jvir.2020.01.028.

3D augmented reality visualization informs locoregional therapy in a translational model of hepatocellular carcinoma

Brian J. Park, MD[1], **Nicholas R. Perkons, BS**[1], **Enri Profka**[1], **Omar Johnson, MS**[1], **Christopher Morley, MD**[2], **Scott Appel, MS**[1], **Gregory J. Nadolski, MD**[1], **Stephen J. Hunt, MD, PhD**[1], **Terence P. Gade, MD, PhD**[1]

[1]Perelman School of Medicine, University of Pennsylvania, 646 BRB II/III, 421 Curie Blvd, Philadelphia, PA, Philadelphia, PA 19104

[2]Medivis, 370 Jay St, Brooklyn, NY, 11201

Abstract

Purpose: To evaluate the utility of visualizing pre-procedure MRI in three-dimensional (3D) space using augmented reality (AR) prior to transarterial embolization (TAE) of hepatocellular carcinoma (HCC) in a preclinical model.

Materials and Methods: A prospective study with a total of 28 rats with diethylnitrosamine (DEN)-induced HCC and tumors greater than 5 mm treated with TAE were included. In 12 rats, 3D AR visualization of the pre-procedure MRI was performed prior to TAE. Procedural metrics including catheterization time and radiation exposure were compared to a prospective cohort of 16 rats in whom TAE was performed without AR. An additional cohort of 15 retrospective cases were identified and combined with the prospective control cohort (n=31) to improve statistical power.

Results: A reduction in fluoroscopy time was observed after AR when compared prospectively from 11.7 to 7.4 min (37%; p=0.12), which did not reach statistical significance; however, when compared to combined prospective and retrospective controls, the reduction in fluoroscopy time was significant from 14.1 to 7.4 min (48%; p=0.01). A reduction in total catheterization time was also observed after AR when compared prospectively from 42.7 to 31.0 min (27%; p=0.11), which did not reach statistical significance. No significant differences were seen in dose area product (DAP) or air kerma (AK) prospectively.

Conclusions: 3D AR visualization of pre-procedural imaging may aid in the reduction of procedural metrics in a preclinical model of TACE. These data support the need for further studies to evaluate the potential of AR on endovascular oncologic interventions.

Corresponding Author: Brian Park MD 700 Commodore Ct Unit 2714 Philadelphia, PA 19146 bjinwoopark@gmail.com cell 815-621-5752 fax 888-722-0453.

Conflicts of Interests and Financial Disclosures: Christopher Morley is the founder and COO of Medivis, which developed 3D AR visualization software used in this study.

Introduction

Augmented reality (AR) is an emerging display technology that can provide stereoscopic 3D views of cross-sectional imaging [1, 2]. The added depth information afforded by stereoscopic 3D AR may inherently enhance and improve functional neural processes for learning and comprehension, consistent with findings demonstrated using 3D printing for surgical planning, which resulted in reduced operating room times and decreased exposure to ionizing radiation [3–5]. Indeed, 3D visualization technologies have been shown to improve anatomic knowledge and test performance in medical students compared to 2D images [6].

Three-dimensional software and systems currently exist for volumetric vasculature reconstruction [7, 8]. However, many of these systems are limited by 3D data reduced to 2D monitor screens and often require separate workstations that are not integrated with live fluoroscopy. With AR headsets, holographic 3D data can be integrated with actual data in the interventional suite. Monitors displaying live digital subtraction angiography can be overlaid with, and matched to, holographic 3D pre-procedural scans to provide depth information that is absent from the angiographic images (Fig. E1 and Video 1).

The feasibility of stereoscopic 3D visualization of cross-sectional imaging for endovascular procedures has been demonstrated using pre-procedural contrast-enhanced CT and time-of-flight MR angiography [7, 9]. However, the influence of 3D visualization using AR headsets on procedure duration and radiation exposure remain to be investigated. This study evaluates the utility of visualizing pre-procedural MRI in 3D space using an AR optical see-through head-mounted display prior to TAE in rats for improving procedural metrics.

Materials and Methods

Study Design

This study was approved by University of Pennsylvania Institutional Animal Welfare & Use Committee. The induction of cirrhosis and HCC in rats using DEN and TAE via right common femoral artery access were previously described [10, 11]. All rats developed tumors, the majority of which appeared within 2 weeks of completing the DEN diet. Rats were serially imaged, and TAE was performed when at least one tumor measured greater than 5 mm in maximum axial diameter. Only one tumor was treated in a single TAE session. TAE was performed by one of two interventional radiologists, each with greater than 5 years of experience working with rats.

A total of 28 prospective cases were enrolled: 12 in the AR group and 16 in the prospective control group from August 2018 to June 2019. Rat population characteristics, including sex, weight, maximum axial tumor dimension, and liver location between the groups were compared (Table 1). Procedural metrics including total catheterization time, total fluoroscopy time, DAP, and AK from prospective TAEs with and without AR were compared. Post-hoc power analysis suggested a total sample size of 52 for 80% power to achieve statistical significance ($\alpha<0.05$) with a large effect size (0.8). Since prospective comparisons were underpowered (n=28), an additional 15 retrospective control cases from

January 2017 to December 2017 were identified. The prospective and retrospective control cases were combined, after being determined to be statistically similar, and compared to the AR group to improve power. Fluoroscopic guidance and angiography for prospective cases were performed on Siemens Cios Alpha (Siemens Healthineers, Erlangen, Germany); retrospective cases were performed on Siemens Siremobil ISO-C. A flowchart of the study design is depicted in Fig. 1.

Transarterial Embolization

Rats were first induced with 2% isoflurane at 1L/min oxygen. Anesthesia was maintained with inhalation through a nose cone of 1.5–2% isoflurane at 1L/min oxygen. The animal was then placed in a supine position on top of a circulating water blanket, which maintained body temperature at 37°C. Body temperature was monitored throughout the procedure using a rectal temperature probe. The right medial thigh and groin were shaved and cleaned with 4% chlorhexidine gluconate solution, and then draped with a sterile cover. A 3 cm incision along the medial thigh was made to reveal the femoral sheath. Using blunt and fine-tipped forceps, the femoral sheath was dissected until the femoral artery was exposed. Afterwards, vessel loops of 5–0 silk suture were placed along the proximal and distal segments of the femoral artery to control blood flow in the exposed segment. Using a Leica M80 stereomicroscope (Leica Microsystems AG, Heerburgg, Switzerland) an arteriotomy was created in the center of the exposed segment using a 26-gauge Angiocath (outer diameter, 0.46 mm; BD Biosciences, San Jose, CA). An 8–0 suture (Fine Science Tools) was placed on one of the lips created by the arterial puncture for the purpose of facilitating the introduction of a catheter. A custom pre-shaped J catheter (Excelsior SL-10 microcatheter, Stryker, Kalamazoo, MI) modified to 30 cm in length was introduced into the femoral artery. The catheter was advanced into the femoral artery with the aid of a coaxially inserted 0.010-inch guidewire (Transend guidewire, Stryker). Then, selective catheterization of the celiac artery and arteriography with Omnipaque 300 (0.3 mL, GE Healthcare, Chicago, IL) were performed. Superselective catheterization of the segmental hepatic artery supplying the tumor was performed using a coaxially inserted SAI MTV-40 microcatheter (SAI Infusion Technologies, Lake Villa, IL). Embolization was performed with either 0.05 mL of sedimented 40–120 (μm Embospheres (Merit Medical Systems, South Jordan, UT) or 40–90 (μm LC Bead LUMI (BTG plc, London, United Kingdom) diluted in 0.9 mL of Omnipaque 300. Delivery of the embolic was achieved using a 1-mL polycarbonate syringe via hand injection or PHD Ultra Syringe Pump (0.15 mL/min rate, Harvard Apparatus, Holliston, MA) injection until the endpoint of embolization was achieved with stasis in the selected segmental hepatic artery. Post-embolization arteriography was performed to confirm stasis. Finally, the catheters were removed, and the 8–0 suture placed on the proximal lip of the arteriotomy was used to close vessel wall. The fascia and skin were then closed with interrupted 5–0 sutures.

In all cases, 2D pre-procedural images were reviewed prior to TAE. In the AR group, pre-procedural AR visualization was additionally performed immediately prior to the start of the procedure. Total femoral artery catheterization time, which includes both nonselective and selective catherization of segmental hepatic arteries; total fluoroscopy time; DAP; and AK were recorded. Total femoral artery catheterization time was used as a proxy for IR-related

procedure time. Microsurgery and cut down to the femoral artery for access and catheter insertion were not included in the procedure time as this time was highly variable and is not applicable to human cases. Additionally, emphasis was placed on procedural-related tasks directly relevant to pre-procedural imaging and the femoral arteries were not included in the pre-procedural MRI of the abdomen. Total femoral artery catheterization time was calculated by the difference from the last fluoroscopic image time to the first fluoroscopic image time. This was validated in 6 prospective cases comparing manually recorded catheterization times to differences in fluoroscopic image timestamps. There was strong correlation between manually recording times to using fluoroscopic image timestamps with Pearson correlation coefficient r=0.99 (Fig. E2).

MRI

Axial and coronal T2-weighted images were acquired using a Varian 4.7 Tesla 40-cm horizontal bore MR spectrometer with a 25 gauss/cm gradient tube interfaced to a Varian Direct Drive console (Agilent Technologies, Santa Clara, CA). Images of the abdomen were acquired from the lung bases to the pelvic inlet and did not include the femoral arteries. Sequence parameters included 70 mm × 70 mm FOV, 2 mm slice thickness, 20 slices, 4 averages, 256 × 256 matrix size, TR 1.5–2 s, and TE 60 ms. Of note, intravenous gadolinium contrast media (total mL with 0.3 mL contrast and 0.7 mL saline) was administered via tail vein and post contrast images were acquired. Rats were anesthetized with isoflurane for the duration of MRI. DICOM images were exported from the scanner, and 2D slices were sequentially reviewed using ITK- SNAP software [12].

3D Holographic Rendering

Holographic 3D volumes were generated using 3D texture mapping of the DICOM dataset. MR T2-weighted images were exported from the scanner in DICOM format. Direct volume rendering was performed using ray casting and optimization techniques using SurgicalAR software (Medivis, Brooklyn, NY) on an Alienware R3 15 laptop with Intel Core i7–7820HK, 32GB RAM, and GTX 1080 GPU. Rendering was performed locally on the laptop and remotely streamed to HoloLens (Microsoft, Redmond, WA) augmented reality headset device in real time via 5Ghz Wi-Fi. Holographic 3D volume manipulations including rotation, magnification, windowing, and modification of voxel opacities were utilized during HoloLens visualization. Additionally, an invisible cut plane at a set distance from the headset allowed the ability to view into the volume from any perspective angle (Video 2). AR system setup and operator viewing times were recorded.

Statistical Analysis

Statistical analysis was performed using Google Sheets software (Google, Mountain View, CA). Means and variances were compared using Welch’s t-test and F-test, respectively. Categorical rat population characteristics were compared using chi-squared test. Outlier analysis was initially performed for values beyond 2 times the interquartile range and omitted from inclusion for comparison. This included the omission of high radiation exposures from one case with AR, including fluoroscopy time, air kerma, and DAP, in which further investigation revealed that settings during the case were unintentionally altered between fluoroscopy and digital radiography. Additionally, high DAP value from one case

without AR was omitted. The reason for this high DAP value was unknown as fluoroscopy time and air kerma values from this case remained within outlier limits.

Results

Procedural metrics from TAEs are summarized in Table 2. AR system setup and operator viewing times measured approximately 3 min each, for an average total of 5.9 min of additional pre-procedure time per case (Fig. 2). Prospective analysis showed a reduction in total catheterization time, including nonselective and selective catheterization, from 42.7 min to 31.0 min after AR that did not reach statistical significance (27%, p=0.11). A reduction in total fluoroscopy time was also observed from 11.7 min to 7.4 min after AR that did not reach statistical significance (37%, p=0.12). As expected with decreased fluoroscopy times, there were associated reductions in DAP and AK prospectively, which did not reach statistical significance. The reduction in DAP was incremental (4%; p=0.83) compared to the reduction in AK (37%, p=0.13).

Comparisons between the prospective and retrospective control groups showed no difference in the mean catheterization or fluoroscopy times despite the 2-year time difference between the groups (p=0.97 and p=0.48, respectively). Additionally, there was no statistically significant difference in the variance in fluoroscopy time between the control groups (p=0.08). Since the mean and variance in fluoroscopy time between the prospective and retrospective control groups were similar, these control groups were combined to improve statistical power. The increase in power afforded by combining these control groups demonstrated a significant reduction in fluoroscopy time after AR from 14.1 to 7.4 min (48%; p=0.01; Fig. 3). In addition, there was a statistically significant difference in the variance in fluoroscopic time prospectively (p=0.02; Table 2) with a reduction in this variation after the use of AR (Fig. 3). The different angiography systems used for the retrospective and prospective control groups confounded comparisons of radiation exposure.

Discussion

Stereoscopic 3D visualization pre-procedurally with AR showed a reduction in fluoroscopy time that did not reach statistical significance when compared to a prospectively acquired control group, likely due to limited statistical power. As such, a statistically significant reduction in fluoroscopy time was observed after the use of AR when compared to combined prospective and retrospective controls. DAP and AK are closely related to fluoroscopy time and expected trends in reductions in these values were also present prospectively but did not reach statistical significance. Despite DAP and AK being complementary, the reduction in DAP was incremental, if any, compared to the reduction in AK. This discrepancy in reduction may be partly related to the fact that rats are small, and TAEs were performed on angiography systems intended for human use and calibrated with human phantoms.

The reduction in total catheterization time, which includes nonselective and selective catheterization, after AR also did not reach statistical significance. In addition to differences in anatomy on a case by case basis, other factors influencing total catheterization time included delivery and type of the embolic. Embolization was either performed with 40–120

μm Embospheres or 40–90 μm LUMI beads, and one may have achieved endpoint of embolization and vessel stasis more quickly than the other. These factors, among others, may have influenced catheterization time.

Although pre-procedural planning time increased slightly with AR, there is potential to have greater savings in catheterization time, a marker of procedure time, as well as fluoroscopy time to outweigh the increased planning time. Consistent with this benefit, AR was associated with a reduction in variations in fluoroscopy time, suggesting that AR may be helpful in preventing excessively high fluoroscopy use. For endovascular procedures, 3D visualization may aid in the understanding of where to precisely position the catheter and result in decreased fluoroscopy times, however actually advancing the catheter to that position may be influenced by a variety of factors that can diminish the associated improvements in procedural metrics, including but not limited to operator experience, available catheters and wires, and angles of branching vessels. Nevertheless, these findings demonstrate potential quantitative and tangible benefits from AR that are necessary to motivate clinical trials.

The potential benefits of 3D AR visualization of pre-procedural imaging prior to TAE may be multifactorial. Three-dimensional AR visualization has been shown to decrease mental task load during simulated surgery [13]. Despite the unknown cognitive mechanism, benefits from holographic 3D visualization could have real value. In addition, the freedom and ease to visualize the volume with AR in any plane and from any perspective angle may provide insight into optimally positioning the C-arm detector during the procedure, thereby decreasing vessel selection time and fluoroscopy time. As shown in Video 2, particularly when the holographic 3D volume is visualized in the coronal orientation, the AR headset can simulate C-arm positioning and help establish relationships of the target relative to the spine or other lesions in the liver. The operator can also obtain a better 3D depiction of the catheter course needed for vessel selection, which may be difficult to ascertain from scrolling through pre-procedural images on a 2D monitor screen. As a result, the operator can not only obtain an improved practical sense of anatomy pre-procedurally, but this greater sense of anatomic understanding in relation to other structures can manifest as an ancillary aid as well as facilitate innate recall during tasks in the procedure. Along these lines, and based on studies using 3D printed models for surgical planning, smoother and faster procedures with decreased fluoroscopy use would be anticipated with improved planning, recall, and anatomic understanding [3–5]. Ultimately, improved anatomic understanding after AR may give the operator enough confidence to forego cone beam CT during the procedure, thereby saving procedure time and radiation exposure. Although AR utilization was only performed in the pre-procedural planning phase, intra-procedural 3D AR may also potentially benefit procedural metrics (Fig. E1 and Video 1).

Limitations of this study include a single-center study and the use of both prospective and retrospective data for analysis. Prospective comparisons showed changes in procedural metrics that did not reach statistical significance. As this study was determined to be underpowered, retrospective controls were analyzed and combined to increase statistical power. Additionally, although the operators may have become more efficient and able to selectively catheterize arteries faster over time with experience, there was no difference in

mean catheterization time or fluoroscopy time between the prospective and retrospective control groups. This absence in improvement argues against benefits from increased operator experience with time. Moreover, both operators have been performing TAEs in rats in a similar fashion since 2014. In addition, implicit bias may exist from merely utilizing AR, which is difficult to control. The possibility remains that by simply donning the headset, the operator may have been compelled to perform the procedure more quickly or use less fluoroscopy. Also, the complexity of the cases was not analyzed or taken into account, for example, variant anatomy or multiple feeding vessels, which would impact catheterization time and fluoroscopy use.

In conclusion, this study suggests that AR may provide immediate benefit in endovascular procedures by enabling reduced, and more consistent, catherization and fluoroscopy times. Further studies should be performed to evaluate the potential of AR on endovascular oncologic interventions.

Supplementary Material

Refer to Web version on PubMed Central for supplementary material.

Acknowledgments:

BP reports grants from the NIH (5T32EB004311), SIR Foundation, RSNA R&E Foundation and Nvidia; and non-financial support from Medivis during the conduct of the study. NP has nothing to disclose. EP has nothing to disclose. OJ has nothing to disclose. CM reports other financial activities from Medivis, Inc. SA has nothing to disclose. GN has nothing to disclose. SH reports personal fees from BTG and Amgen outside the submitted work. TG reports personal fees from Trisalis Life Sciences outside the submitted work. Special thanks to the Penn Medicine Medical Device Accelerator for supporting equipment for this research.

SIR Annual Scientific Meeting: Park B, Perkons N, Profka E, Morley C, Nadolski G, Hunt S, Gade T. Outcomes from 3D augmented reality visualization for transarterial embolization in rats. E-poster at SIR 2019, Austin, TX. 26 Mar 2019.

References

[1]. Sutherland J, Belec J, Sheikh A, et al. Applying Modern Virtual and Augmented Reality Technologies to Medical Images and Models. J Digit Imaging 2018; 32:38–53.

[2]. Uppot RN, Laguna B, McCarthy CJ, et al. Implementing Virtual and Augmented Reality Tools for Radiology Education and Training, Communication, and Clinical Care. Radiology 2019:182210.

[3]. Mitsouras D, Liacouras P, Imanzadeh A, et al. Medical 3D Printing for the Radiologist. Radiographics 2015; 35:1965–88. [PubMed: 26562233]

[4]. Tack P, Victor J, Gemmel P, Annemans L. 3D-printing techniques in a medical setting: a systematic literature review. Biomed Eng Online 2016; 15.

[5]. Perica ER, Sun Z. A Systematic Review of Three-Dimensional Printing in Liver Disease. J Digit Imaging 2018; 31:692–701. [PubMed: 29633052]

[6]. Yammine K, Violato C. A meta-analysis of the educational effectiveness of three-dimensional visualization technologies in teaching anatomy. Anat Sci Educ 2015; 8:525–38. [PubMed: 25557582]

[7]. Mohammed MAA, Khalaf MH, Kesselman A, Wang DS, Kothary N. A Role for Virtual Reality in Planning Endovascular Procedures. J Vasc Interv Radiol 2018; 29:971–4. [PubMed: 29935787]

[8]. Miyayama S, Yamashiro M, Sugimori N, Ikeda R, Okimura K, Sakuragawa N. Outcomes of Patients with Hepatocellular Carcinoma Treated with Conventional Transarterial Chemoembolization Using Guidance Software. J Vasc Interv Radiol 2019; 30:10–8. [PubMed: 30580809]

[9]. Karmonik C, Elias SN, Zhang JY, et al. Augmented Reality with Virtual Cerebral Aneurysms: A Feasibility Study. World Neurosurg 2018; 119:e617–e22. [PubMed: 30077029]

[10]. Gade TP, Hunt SJ, Harrison N, et al. Segmental Transarterial Embolization in a Translational Rat Model of Hepatocellular Carcinoma. J Vasc Interv Radiol 2015; 26:1229–37. [PubMed: 25863596]

[11]. Kiefer RM, Hunt SJ, Pulido S, et al. Relative Initial Weight Is Associated with Improved Survival without Altering Tumor Latency in a Translational Rat Model of Diethylnitrosamine- Induced Hepatocellular Carcinoma and Transarterial Embolization. J Vasc Interv Radiol 2017; 28:1043–50 e2. [PubMed: 28495453]

[12]. Yushkevich PA, Piven J, Hazlett HC, et al. User-guided 3D active contour segmentation of anatomical structures: significantly improved efficiency and reliability. NeuroImage 2006; 31:1116–28. [PubMed: 16545965]

[13]. Fotouhi J, Fuerst B, Lee SC, et al. Interventional 3D augmented reality for orthopedic and trauma surgery. Int Society for Computer Assisted Orthopedic Surgery, 2016.

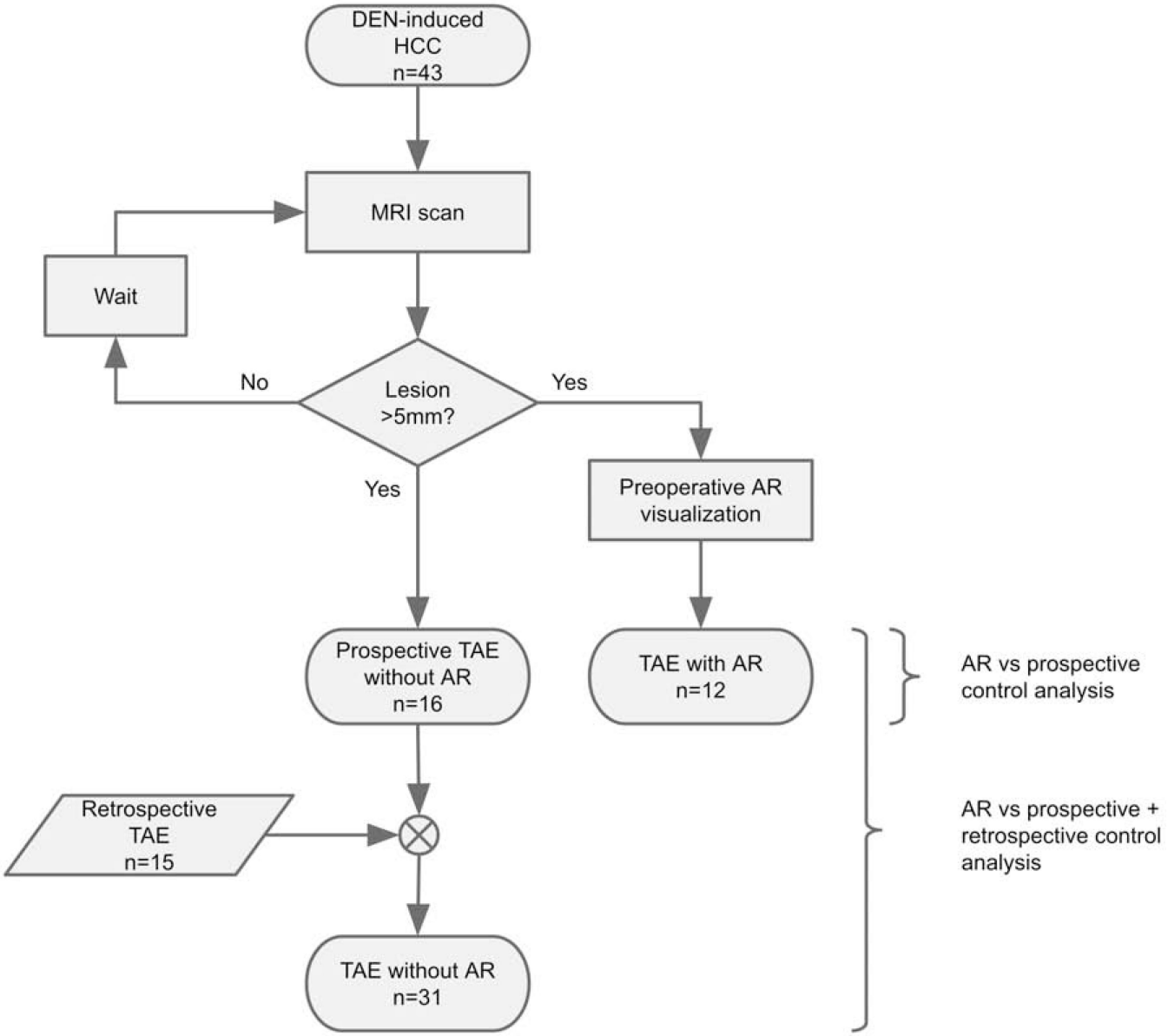

Figure 1.

Flowchart of study design. Prospective analysis was performed with and without AR. Retrospective controls were added to improve statistical power and analyzed separately.

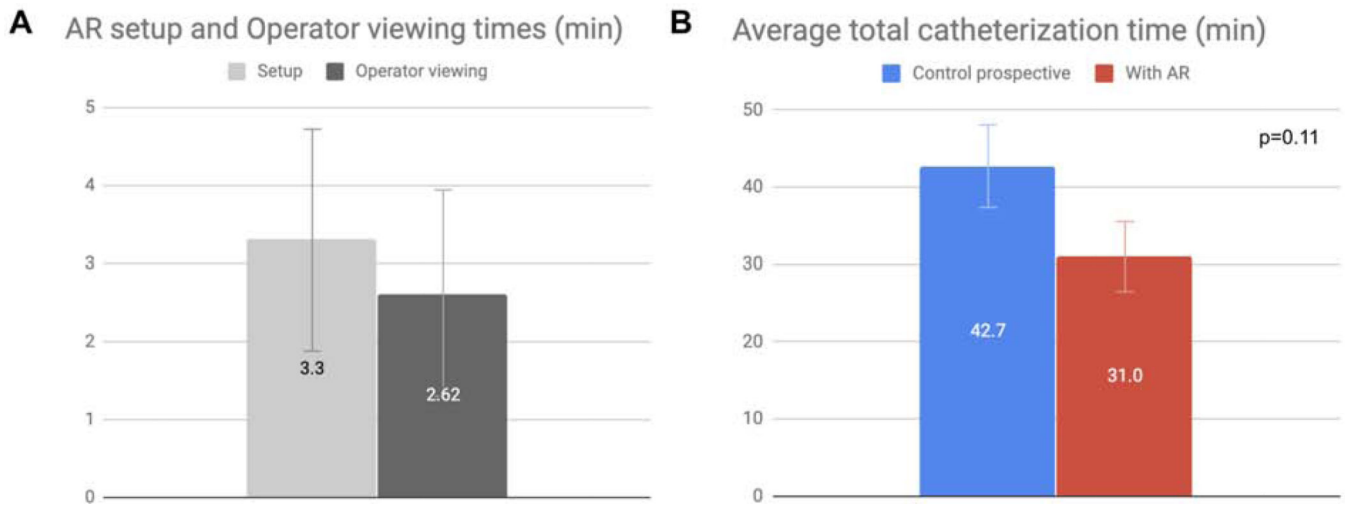

Figure 2.

Bar graphs of AR system setup and operator viewing times as well as total catheterization times for prospective TAEs performed with and without AR. A. Setup and operator viewing times were similar. Error bars represent standard deviation. B. 27% decrease in average total catheterization time (p=0.11). Error bars represent standard error from the mean.

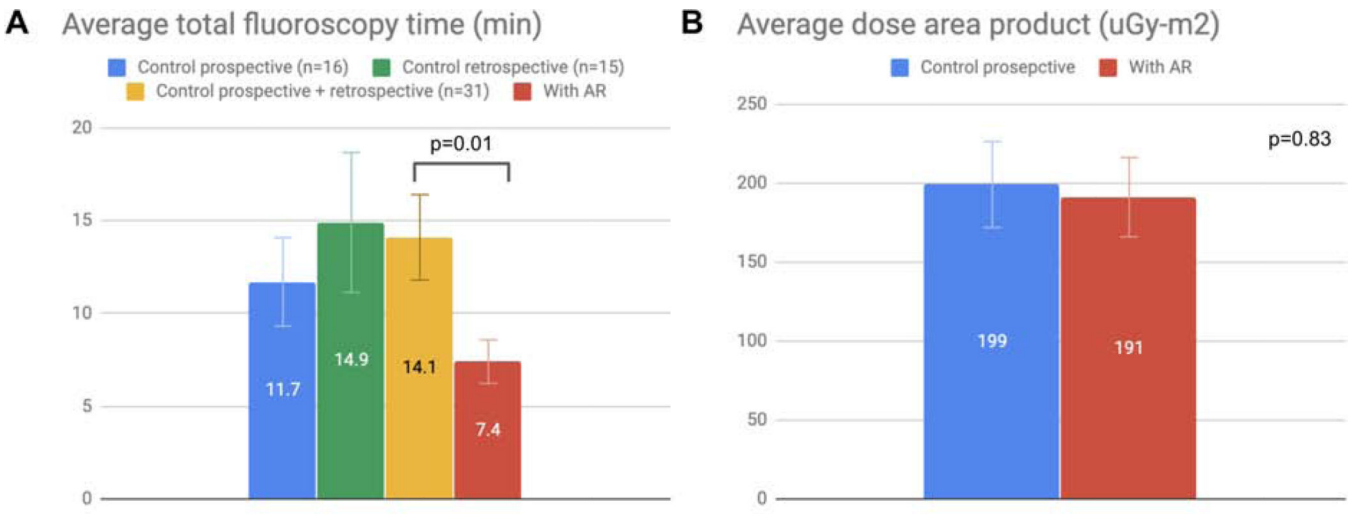

Figure 3.

Bar graphs of radiation exposure for TAEs performed with or without AR. Error bars represent standard error from the mean. A. 36% decrease in total fluoroscopy time with AR compared to prospective controls (p=0.12). No difference in fluoroscopy time between prospective and retrospective controls (p=0.48). 48% decrease in fluoroscopy time compared to combined prospective and retrospective controls (p=0.01). Variation narrowed following AR as seen in the error bars. B. No significant change in DAP was observed (p=0.83) despite decreased fluoroscopy time.

Table 1.

Summary of rat population characteristics.

	Control prospective	**AR**	***P***
n	16	12	
Sex	16 male	12 male	
	0 female	0 female	
Avg weight (g)	428	464	0.08
Liver location	12 left	8 left	0.82
	5 right	4 right	
Avg tumor max axial dimension (mm)	10.2	8.4	0.28

Table 2.

Summary of procedural metrics from TAE in rats with and without AR utilization.

	AR	Control prospective	T-test	F-test
n	12	16		
Avg HoloLens setup time (min:sec)	3:22	--		
Avg HoloLens utilization time (m:s)	2:52	--		
Avg total cath time (min)	31.0	42.7	0.11	0.21
Avg total fluoro time (min)	7.4	11.7	0.12	0.02*
Avg DAP (uGy-m2)	191	199	0.83	0.31
Air Kerma (mGy)	17.6	28.0	0.13	0.01*

	AR	Control retrospective	T-test	F-test
n	12	15		
Avg total cath time (min)	31.0	42.3	0.41	0.001*
Avg total fluoro time (min)	7.4	14.9	0.08	0.002*
Avg DAP (uGy-m2)	191	302	0.051	0.03*
Air Kerma (mGy)	17.6	81.6	0.001*	0.0001*

	Control prospective	Control retrospective	T-test	F-test
n	16	15		
Avg total cath time (min)	42.7	42.3	0.97	0.004*
Avg total fluoro time (min)	11.7	14.9	0.48	0.08
Avg DAP (uGy-m2)	199	302	0.07	0.04*
Air Kerma (mGy)	28.0	81.6	0.003*	0.003*

	AR	Control combined prospective and retrospective	T-test	F-test
n	12	31		
Avg total cath time (min)	31.0	43.1	0.12	0.01*
Avg total fluoro time (min)	7.4	14.1	0.01*	0.004*
Avg DAP (uGy-m2)	191	251	0.13	0.05*
Air Kerma (mGy)	17.6	56.9	0.0002*	0.0002*

* $p < 0.05$